Available online at www.sciencedirect.com

ScienceDirect

Advances in Space Research 71 (2023) 3468–3478

ADVANCES IN SPACE RESEARCH (a COSPAR publication)

www.elsevier.com/locate/asr

Study of Neptune dayside magnetosheath fluctuations during Voyager-2 flyby

Ezequiel Echer [a,*], Adriane Marques de Souza Franco [b], Fabíola Pinho Magalhães [c], Mauricio J.A. Bolzan [d], Rajkumar Hajra [e]

[a] Instituto Nacional de Pesquisas Espaciais (INPE), São José dos Campos, Brazil
[b] Federal University of Southern and Southeastern Pará, Marabá, Brazil
[c] Independent Researcher, Florianópolis, Brazil
[d] Federal University of Jatai, Jatai, Brazil
[e] Indian Institute of Technology Indore, Indore 453552, India

Received 21 May 2022; received in revised form 17 November 2022; accepted 9 December 2022
Available online 28 December 2022

Abstract

Turbulence in the outer planetary magnetospheres has been relatively less studied than in the Earth's magnetosphere, especially for the ice giants which have been visited only by the Voyager-2 spacecraft so far. The aim of this work is to study the turbulence in Neptune's dayside magnetosheath. Voyager-2 magnetometer 3-s averaged magnetic field data were analyzed with several data analysis techniques. It was found that most of the magnetosheath magnetic field is aligned in the B_T direction. The B_R-component spectrum showed the predominance of short-period (5 minutes) oscillations, while the B_T- and B_N- components showed the occurrence of longer-period (20–50 minutes) oscillations. The Fourier spectrum of the magnetic field showed a breakpoint near 0.00165 Hz. The lower frequency portion showed index (absolute values) smaller than 1.0. The higher frequency portion showed a much steeper spectrum, with power law values varying from about 2.0 to 2.4. The statistical kurtosis parameters for B_R and B_N are higher than 3 in almost all scales, while the B_T component (main field direction) has a more Gaussian or sub-Gaussian behavior, specially in scales higher than 20 minutes. The kurtosis is very high at the low frequency spectral power of 40 minutes for the B_N-component, indicating asymmetric or non-Gaussian magnetic field distribution in the magnetosheath. The multifractal spectrum is well spread in the magnetosheath revealing a rich and dynamic activity in this region. Overall, the Neptune's magnetosheath is found to have a strong turbulence activity that is comparable to that of other planetary magnetosheaths.

Keywords: Neptune; Voyager; Solar wind; Waves; Turbulence; Magnetosheath

1. Introduction

The Neptune system has been explored in situ so far only by the Voyager-2 spacecraft (Russell and Luhmann, 1997). It was found that Neptune has a large magnetosphere and its dipole magnetic field has an offset of 47° with respect to its rotation axis. Closer to the planet, higher order magnetic multipoles are important (Ness et al., 1989; Zhang et al., 1991; Russell and Walker, 1995; Russell and Luhmann, 1997; Kivelson and Bagenal, 1999). This large magnetic dipole inclination, combined with the 29° tilt of its rotation axis to the ecliptic plane, cause a variation in its magnetosphere from Earth-like to near pole-on configuration. As a consequence, Voyager-2, during its 1989 flyby, encountered the polar cusp magnetosphere of Neptune (Ness et al., 1989; Russell and Luhmann, 1997).

* Corresponding author.
E-mail address: ezequiel.echer@gmail.com (E. Echer).

https://doi.org/10.1016/j.asr.2022.12.022
0273-1177/

The closest approach of Neptune by Voyager-2 occurred on 25 August 1989 (Ness et al., 1989). The inbound bow shock was crossed by Voyager-2 at 34 Neptune radii (1 $R_N = 24,622$ km) at ~14:30 UT on 24 August (Szabo and Lepping, 1995; Richardson et al., 1994). The inbound magnetopause was observed at ~18:00 UT on 24 August, but extended in a long-interval observed in several instruments because of the complex nature of the magnetopause. It was not as sharp as expected because Voyager-2 was entering the magnetosphere through the south polar cusp (Ness et al., 1989; Zhang et al., 1992). According to Szabo and Lepping (1995), the solar-wind condition was steady for several hours before the bow shock crossing. Neptune's bow shock was characterized by a low upstream thermal proton plasma-β of 0.04 (β is defined as the ratio of the plasma thermal pressure to the magnetic pressure), a high magnetosonic Mach number, M_{ms} of ~8.8 (M_{ms} is the ratio of the solar-wind speed to the local magnetosonic speed), and quasi-perpendicular orientation (shock normal angle θ_{Bn} of 59^o) to the ambient interplanetary magnetic field (IMF) (Richardson et al., 1994; Szabo and Lepping, 1995). In the magnetosheath, the plasma bulk velocity dropped to submagnetosonic values ($M_{ms} < 1$), the density and magnetic field increased significantly, and fluxes of heated electrons and ions were observed (Richardson et al., 1994; Zhang et al., 1992).

The planetary magnetosheath is a region between the bow shock and the planetary magnetospheric boundary (magnetopause or magnetospheric boundary layer), where the solar wind is compressed, decelerated, deflected and heated. As a result, this region is permeated by solar wind turbulence (Fairfield, 1976; Kivelson and Bagenal, 1999; Richardson, 2002; Remya et al., 2013; Bolzan and Echer, 2014; Franco et al., 2020; Saur, 2021). The main propagation modes observed in the planetary magnetosheath are the mirror mode oscillations and the ion-cyclotron waves (Tsurutani et al., 1982; Richardson, 2002; Tsurutani et al., 2011). The mirror mode oscillations are pressure balanced structures, with decreases in the magnetic field magnitude but without significant variation in the angular magnetic coordinates (Tsurutani et al., 1982; Richardson, 2002; Tsurutani et al., 2011). They are thought to be generated by ion instability due to temperature anisotropy. Their quasi-periodical appearance in the spacecraft frame is due to the solar-wind convection, as they are non-propagating structures (Tsurutani et al., 2011). On the other hand, the ion-cyclotron waves arise from the resonant wave-particle interactions, where waves gain energy from particles. Charged particles are scattered by wave fields, and particle's momentum and energy change through this process (Hasegawa, 1969; Fairfield, 1976; Tsurutani et al., 1982; Tsurutani and Lakhina, 1997; Richardson, 2002; Tsurutani et al., 2011).

Outer planet magnetosheath turbulence has been relatively less studied than Earth's magnetosheath, especially Neptune and Uranus, which have been so far explored only by the Voyager-2 spacecraft (Saur, 2021, and references therein). For instance, Echer (2009) studied the magnetic field fluctuations in Neptune's magnetosheath using wavelet analysis. He found high-frequency (~3–5 minutes) fluctuations near the bow shock, and low-frequency (~10–20 minutes) oscillations near the magnetopause. These structures were found to be broader, lower in frequency, and stronger in amplitude going from the bow shock to the magnetopause, with periods longer than the proton-gyro period (96 seconds during that period).

The aim of this work is to perform a detailed analysis of the fluctuations in the Neptune dayside magnetosheath. Several data analysis techniques will be employed in this work: Fourier analysis, Lomb-Scargle periodogram, kurtosis and multifractal analyses, in order to characterize and quantify the turbulence in this space plasma environment. The resultsobtained will be compared with previous works on other planetary magnetosheaths.

2. Data and methodology

2.1. Voyager-2 magnetic field data

The magnetic field near Neptune space environment was measured by a triaxial fluxgate magnetometer onboard the Voyager-2 spacecraft (Behannon et al., 1977; Ness et al., 1989). The 1.92-second resolution data were collected from NASA's Planetary Data System (http://pds.jpl.nasa.gov; McMahon, 1996). The high-resolution magnetic field data were averaged to a resolution of 3 seconds in order to have a homogeneous data set. The few remaining gaps were removed with linear or spline interpolation. The magnetic field is given in the spacecraft centered radial-tangential-normal (RTN) heliographic coordinates, where the magnetic field vector is expressed in the radial (B_R), tangential (B_T) and normal (B_N) components. In this system, $\mathbf{R}$ is a unit vector directed from the Sun to the spacecraft, $\mathbf{T} = (\Omega \times \mathbf{R})/|(\Omega \times \mathbf{R})|$, where Ω is the Sun's spin axis, and $\mathbf{N}$ completes the right-handed triad.

2.2. Analysis techniques

As mentioned before, several analysis techniques have been employed in this work. They are described briefly below. To analyze the Neptune's bow shock, the magnetic *coplanarity* technique was employed to the measured magnetic field data. It used magnetic field vector data averaged upstream and downstream of a shock to determine its normal vector. A detailed description of this technique can be found in literature (e.g., Echer, 2019, and references therein).

The classical *cross-correlation* technique was employed to study the correlation among the magnetic field vector components as a function of the time lags (Davis, 2002). This technique has widely been used to study the temporal variations of the relation between two time series (e.g., Hajra et al., 2021, and references therein). The correlation technique provides the degree of similarity between two

time series, as well as the lag in time between them. The correlation coefficient varies from −1 (maximum anti-correlation) to 1 (maximum correlation), and it is zero when there is no correlation between the two time series.

To detect periodicities in the magnetosheath wave activity, we employed the *Lomb-Scargle* (LS) periodogram analysis (Lomb, 1976; Scargle, 1982), which estimates the power spectrum of time series in unevenly-sampled observations (for more informations: Horne and Baliunas, 1986; Press and Rybicki, 1989; Baluev, 2008; Zechmeister and Kürster, 2009; VanderPlas and Ivezić, 2015; VanderPlas, 2018). In the power spectrum, it is common to observe the presence of multiple and significant peaks caused by the presence of more than one periodic signal in the data. Scargle (1982) suggested that when the modified periodogram is normalized by a factor of the total variance, at any particular frequency, and in the case of a null hypothesis, the value of the power spectrum has an exponential distribution with unit mean. This exponential distribution is the basis of the *False Alarm Probability* (FAP) formula. This statistical analysis aims to evaluate the significance of the highest peak detected in the periodogram. As a consequence, the peak statistical significance is high if the FAP returns a low or a very low value.

To study the plasma turbulence, the *Fourier power law* analysis, *kurtosis* and *multifractal* techniques were employed. The Fourier spectrum of the time series data is fitted by a power law function. The associated power index is widely used in turbulence studies to characterize the plasma wave activity domains, as well as turbulent activity dependence on the system scales or frequencies of oscillations in the system (Bracewell, 2014; Bolzan and Echer, 2014; Echer and Bolzan, 2016). In the subject of power spectrum analysis of turbulence cascade, seminal work has been done by Kolmogorov (1941, 1962) and Obukhov (1962). In turbulent fluids and plasmas, the large-scale structures contain most of the energy of the system. From there, energy follows a cascade to lower scales by inertial and inviscid mechanisms. This process continues creating smaller structures until the kinetic scales where viscous dissipation of energy happens. This energy cascade is described by a power law of the Fourier spectrum of the time series versus frequency and it usually follows a $-5/3$ dependence law (Kolmogorov law) (Kolmogorov, 1941; Kolmogorov, 1962; Obukhov, 1962). Other important works in the magnetohydrodynamics (MHD) turbulence were developed by Iroshnikov (1963), Kraichnan (1965) who derived a power spectrum with a $-3/2$ dependence law for turbulence. For more details on this topic, we refer the book by Frisch (1995), and references therein.

The intermittent nature of any physical quantity can be investigated through the *Probability Density Function* (PDF) of a set of two-point difference in time-series. For ordinary hydrodynamic or MHD fluids, intermittency appears in the heavy tails of the distribution functions at moderate scales, implying non-Gaussian statistical behavior of the systems. The kurtosis of a normal or Gaussian distribution is equal to 3 (Frisch, 1995; Franco et al., 2021). Thus, a method to quantify the deviation from the Gaussian distribution is given by the computation of kurtosis, defined by:

$$K_r = \frac{< \delta f_r^4 >}{< \delta f_r^2 >^2}, \tag{1}$$

where $\delta f_r = f(t) - f(t+r)$ is the fluctuation obtained through computation of differences in the time series, t is time, and r is the increment factor (integer number).

The multifractal analysis (Arneodo et al., 1995; Bolzan and Echer, 2014) was also employed in this work in order to obtain the singularity spectrum from the data sets. In this work, we used the wavelet transform modulus maxima (WTMM) (Muzy et al., 1991). The WTMM method provides the partition function over the modulus maxima of the wavelet transform (WT) of a time series (Bolzan et al., 2013). The WT of the time series is given by:

$$WT[f(t)](a,b) = \frac{1}{\sqrt{a}} \int_{-\infty}^{\infty} f(t)\psi^*\left(\frac{t-b}{a}\right)dt, \tag{2}$$

where $f(t)$ is the time series, ψ^* is the complex conjugate of a continuous wavelet function ψ, $a > 0$ is the scaling factor controlling the dilation of the mother wavelet, and b is the translation parameter determining the shift of the mother wavelet. Further, the WT can reveal the local characteristics of $f(t)$ at a point t_0. Thus, we have the following power-law relationship:

$$WT[f(t)](a,t_0) \sim |a|^{\alpha(t_0)}, \tag{3}$$

where $\alpha(t_0)$ is the singularity strength, called Hölder exponent. $\alpha(t_0)$ can be obtained through the log–log plot of the WT amplitude versus the scale a. However, this power-law relation is not easy to obtain when the process is given by a hierarchical distribution of singularities, making difficult the accurate acquisition of α on a finite range of scales. The reason is that at a given scale a, each one of the WTMM bifurcates into two new maxima, giving rise to a rich multiplicative cascade in the limit $a \to 0$. A method to solve this problem is to identify a space-scale partitioning over the maxima distribution. Then it is important to use the thermodynamic approach such as the partition function. Thus, we define a partition function, which scales, in the limit $a \to 0$, as (Muzy et al., 1991):

$$Z(a,q) = \sum_n |WT[f(t)](a,t_n)|^q \sim a^{\tau(q)}, \tag{4}$$

where t_n is the position of all local maxima at a fixed scale a, and q is the moment of the measure distributed on the WTMM hierarchy used to define the power-law scaling of $Z(a,q)$. This process provides the power-law for small α of the scaling exponents $\tau(q)$, which is the multifractal spectrum (Muzy et al., 1991).

Recent studies showed that fluctuation distributions of a geophysical time series cannot be well approximated by a Gaussian distribution (see Bolzan and Echer, 2014, and references therein). Further, the so-called "fat tails" in

the probability density function are the characteristics of the multifractal process. Several works have been conducted on multifractal analysis of solar wind turbulence (Wan et al., 2016; Chhiber et al., 2021; Cuesta et al., 2022). Intermittence in the interplanetary medium from 0.16 to 10 AU heliocentric distance was studied with spacecraft in situ measurements by Cuesta et al. (2022). Those authors concluded that lower Reynold number at a fixed physical scale has effects on average lower kurtosis, implying less intermittent behavior. In another study of solar wind turbulence near Solar Probe orbit perihelion, the multifractal analysis was employed by Chhiber et al. (2021). Those authors found that their results support multifractal scaling in the inertial range, and monofractal but non-Gaussian scaling in the subproton range. In a simulation using kinetic approach in 2D and 3D, results showed the development of turbulent coherent structures, and multifractal intermittency in the kinetic range was observed (Wan et al., 2016). The behaviour on the tail of the PDF can be connected to the multifractal processes and the turbulent cascade (Kolmogorov, 1962; Obukhov, 1962).

The *p*-model, which is an algorithm based on the multiplicative cascading method, is successfully applied to simulate the energy dissipation field in turbulent flows (Meneaveau and Sreenivasan, 1987). In the present work, the *p*-model was employed in order to compare the theoretical and experimental singularity spectra. Thus, this model gives us the information about the degree of multifractality of the time series using a simple parameter P that can be used to quantify the spectral width of the process. The singularity exponents h and their Hausdorff dimensions $D(h)$ are related to each other via the non-linear relations (Halsey et al., 2018):

$$h = -\frac{w\log P + (1-w)\log(1-P)}{\log 2} \tag{5}$$

$$D(h) = -\frac{w\log w + (1-w)\log(1-w)}{\log 2} \tag{6}$$

The range $\mu = \alpha_{max} - \alpha_{min}$ quantifies the fractal non-uniformity and is also related to the intermittence degree, i.e., μ is an indicative of the strength of the multifractality of the physical system (Oswiecimka et al., 2006). A single value α for the multifractal spectrum indicates that the signal has a monofractal structure; while multiple values of α indicate that the underlying process is multifractal (Oswiecimka et al., 2006).

3. Results and discussions

3.1. Statistical analysis of the Voyager-2 measurements

Fig. 1 shows the Voyager-2 spacecraft 3-s averaged magnetic field vector components B_R, B_T and B_N, and magnitude $[B_0]$ for the period ~ 14:24–19:12 UT on 24 August 1989. The bow shock and magnetopause crossings are indicated by the vertical dotted and continuous lines, respectively. The selected magnetosheath interval is marked with a red horizontal double-arrow line. The solar-wind background (upstream) was very quiet with B_0 of ~ 0.25 nT and steady field components. The bow shock was detected at ~14:30 UT as an abrupt jump in B_0 and with the start of large oscillations in the field components. The highly fluctuating magnetic field is seen through the whole magnetosheath up to the magnetopause crossing, observed at ~18:00 UT. The magnetopause crossing shows large deflections in magnetic field polarity and a further increase in B_0.

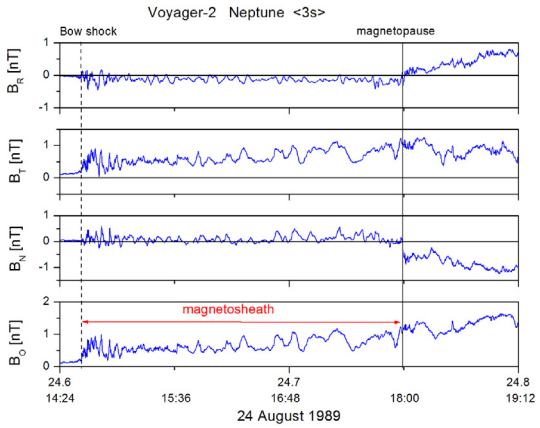

Fig. 1. The Voyager-2 magnetometer data during the Neptune flyby on 24 August 1989. Vertical dotted and continuous lines show the bow shock and magnetopause crossings, respectively. The double-sided red color arrow show the selected magnetosheath interval for this study. The x-axis gives the time in UT and in fraction of day 24 August 1989. (For interpretation of the references to colour in this figure legend, the reader is referred to the web version of this article.)

Using the magnetic coplanarity technique, we computed the bow shock normal. We have found a quasi-perpendicular shock with a shock normal angle $\theta_{B_n} = 57°$, and a compression ratio $r_{B_0} = B_{02}/B_{01} = 3.1$. B_{01} and B_{02} are average B_0 upstream and downstream of the shock, respectively. These results are in agreement with previous works (Richardson et al., 1994; Szabo and Lepping, 1995) reporting an inbound quasi-perpendicular, and strong bow shock with a θ_{B_n} of 59° and a M_{ms} of ~ 9. Further, Szabo and Lepping (1995) found that the bow shock was moving with a speed of 14 km s^{-1} outward of Neptune, with a plasma density compression ratio of 4.2.

Fig. 2 shows the magnetic field latitudinal angle θ_B (defined as $cos^{-1}(B_N/B_0)$, azimuthal angle ϕ_B ($tan^{-1}(B_T/B_R)$), and B_0 for the magnetosheath interval (from the bow shock to the magnetopause). Large variations were noted in θ_B and ϕ_B. It is known that variations in magnetic field angular coordinates are very small for the mirror modes (e.g., Tsurutani et al., 2011). Further, Alfvén waves are known to show very little fluctuations in the magnetic field magnitude and large variations in the components (Bittencourt, 2010). In this case we note very large variations in both components and magnitude. The observed proton cyclotron wave period was 96 seconds, computed for proton

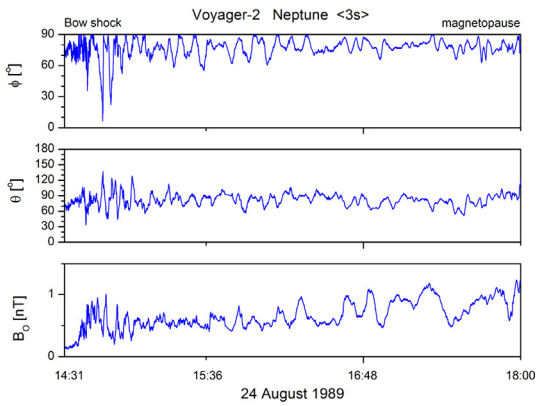

Fig. 2. Neptune magnetosheath magnetic field angular coordinates θ_B and ϕ_B, and magnetic field magnitude B_0.

gyroradius from the ambient magnetic field. Thus the wave periodicities found are well above the kinetic range and in the MHD range. Unfortunately, we did not find high resolution Voyager-2 plasma data for this magnetosheath interval. Therefore we could not check the Alfvénicity by computing the correlation between plasma and magnetic field components. However, the behaviour of the magnetic field oscillations and the proton gyrofrequency value seem to indicate that these waves are most likely fast magnetosonic ion cyclotron waves instead of mirror mode or Alfvénic oscillations. Further, large-amplitude variations are observed in ϕ_B and in θ_B near the bow shock. This is indicative of high-frequency oscillations in the magnetic field components. As the magnetic field oscillations became of lower frequency, these abrupt magnetic field polarity changes decrease from the middle to the end of the magnetosheath.

In the Neptune dayside magnetosheath, most of the field was oriented in the B_T-direction (Fig. 1) due to the deflection of the magnetic field around the Neptune's magnetopause in the dayside magnetosheath. Table 1 shows the statistics of magnetic field parameters. It can be noted that mean B_T is very close to the mean total field B_0 value while other component values are much smaller, close to zero. The variance is also higher in the B_T direction, showing the compressional nature of these fluctuations. The variance is 6 and 3 times higher in the B_T and in the B_N directions, respectively than in the B_R component.

Table 1
Magnetic field parameters for the magnetosheath of Neptune. Rows 2 to 5 give the average ± standard deviation and median values in the parentheses for the magnetic field components. Rows 6 to 8 give the mean variances of the magnetic field components.

Interval/parameter	Magnetosheath
Interval	14:40–18:00
B_0 [nT]	0.682 ± 0.205 (0.618)
B_R [nT]	−0.13 ± 0.082 (−0.1357)
B_T [nT]	0.642 ± 0.206 (0.587)
B_N [nT]	0.0963 ± 0.137 (0.077)
$\sigma^2_{B_R}$ [nT^2]	0.006724
$\sigma^2_{B_T}$ [nT^2]	0.042436
$\sigma^2_{B_N}$ [nT^2]	0.018769

Table 2 shows the linear correlation coefficients (r) between the magnetic field components. The correlation is very high between B_0 and B_T, the field component which contains most of the magnetic field strength, as expected. The correlation is very low between the field magnitude and its transverse components as expected. Further, it can be seen that the correlation coefficient is very low among the magnetic field vector components. The larger correlation between the components is seen between B_T and B_N but with a very low correlation coefficient ($r = 0.21$).

3.2. Periodicity analyses

Periodic fluctuations in the magnetosheath interval are investigated by the Lomb-Scargle technique. The aim is to identify the main periods of the magnetic field fluctuations in the Neptune dayside magnetosheath.

Fig. 3 shows the Lomb-Scargle periodogram of the magnetosheath magnetic field components (B_R, B_T, B_N) and magnitude (B_0). The FAP values obtained are shown by the horizontal dotted lines, with confidence levels from 0.1 to 0.001. Major peaks are indicated with red labels.

The B_R component shows the predominance of periods shorter than 10 minutes. The B_T component shows major peaks at 31 and 51 minutes, while the B_N component shows the predominance of low-frequency periods around 25 and 45 min. Other short periods of about 10 to 15 min are also noted in these components but with lower amplitudes. It can also be seen that the spectrum and major peaks for the field magnitude and B_T are quite similar, as expected, because the magnetic field is oriented toward this component direction.

In the wavelet analysis performed by Echer (2009), it was found that the B_R spectrum shows 3–12 minute periodicities, which were stronger near the bow shock. The B_T wavelet spectrum showed high frequency 3–6 minute oscillations near the bow shock, and continuous 5–15 minute oscillations, from the half of the interval to the magnetopause, and 25 minute oscillations in the 2nd half of the interval. Finally the B_N wavelet spectrum showed 1–5 minute oscillations near the bow shock, quasi-continuous 5–15 minute oscillations, which had largest amplitude close to the magnetopause, and 15–20 minute oscillations near

Table 2
Linear correlation coefficients (r) between the magnetosheath magnetic field components

	Magnetosheath			
	B_R	B_T	B_N	B_0
B_R	1.0	−0.132	−0.03	−0.215
B_T	−0.132	1.0	0.215	0.981
B_N	−0.03	0.215	1.0	0.313
B_0	−0.215	0.981	0.313	1.0

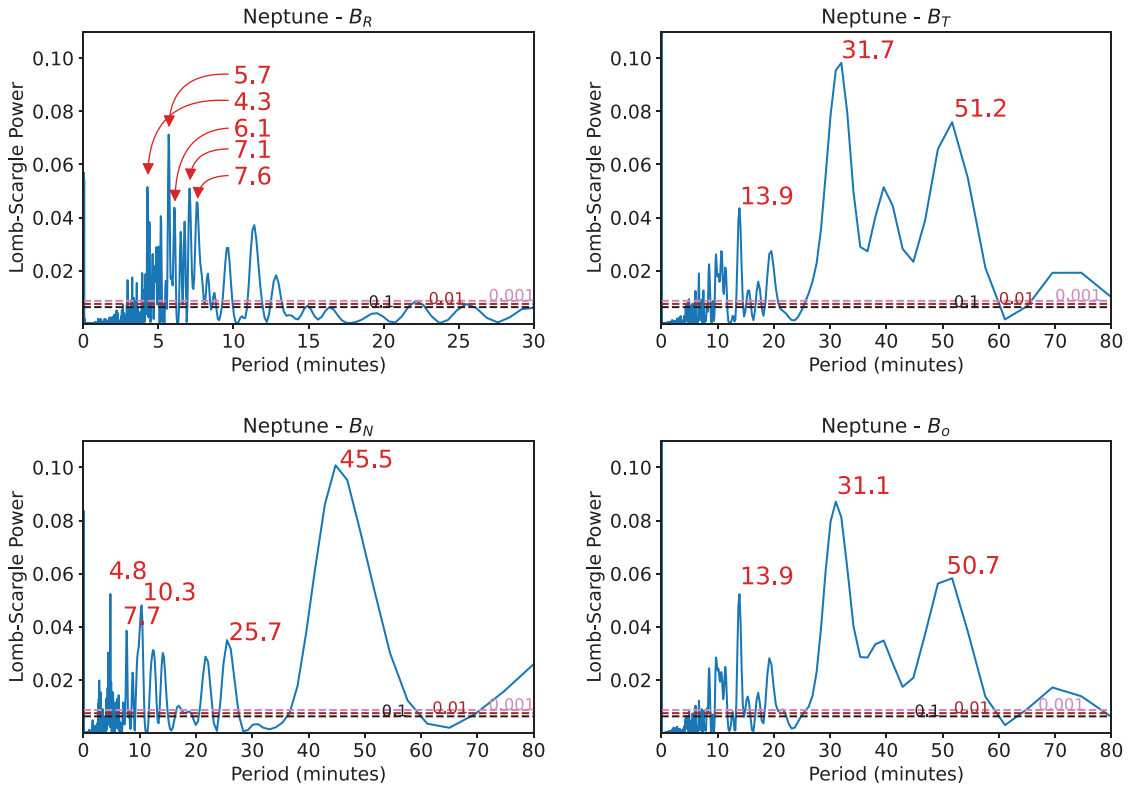

Fig. 3. Lomb-Scargle periodograms of the magnetic field components B_R, B_T and B_N and the magnitude B_0 for the magnetosheath interval. The most significant periods are indicated. Horizontal lines indicate FAPs: 0.1, 0.01, 0.001.

the magnetopause. While the Lomb-Scargle results in this paper are in agreement with the Echer (2009) study, the longer than 30 minute periodicities were not detected in the wavelet analysis by Echer (2009), probably because of the limits of the wavelet cone of influence. There is the predominance of high-frequency oscillations near the bow shock and the lower-frequency fluctuations from the middle of the magnetosheath to the magnetopause. As the proton gyroperiod for this interval is about 1.5 minutes (96 seconds), these oscillations are much longer and well in the MHD regime.

3.3. Intermittence and turbulence analyses

The intermittence in the magnetosheath is studied with the Fourier power law spectrum. Fig. 4 shows the Fourier spectrum (blue lines) and the power law fits (black lines for the low frequency and red lines for the high frequency ranges) of the magnetic field vector components and magnitude in the magnetosheath interval.

The Fourier spectrum of the time series data is fitted by a power law function as: $P = cf^{\alpha}$, where P is the Fourier spectral power, c is a constant, f is the frequency, and α is the power law index. The spectral indices are obtained by the power law fitting (shown by red lines) of the variation of the power spectral density (PSD) with frequency. The spectrum breakpoint was noted at about 0.00165 Hz. For the low-frequency portion, the power law index coefficients are close or below −1.0. The higherindex values in absolute terms are the B_T component and then the B_N, corresponding to the magnetic field direction. For the high frequency range, power index values are much higher, being −2.4 and −2.3 for B_T and B_N and −1.9 for B_R. For the magnetic field magnitude the index is also high, −2.4.

This is coherent with the results shown in Table 1 showing lower B_R variance than the B_T and B_N variances in the magnetosheath. Thus, the higher spectral indices in the magnetosheath are indicative of the larger turbulence in this shocked solar wind plasma region between the bow shock and the magnetopause compared to the ambient solar wind. This higher turbulence is associated with the large amplitude low-frequency oscillations seen in the magnetosheath.

These results are similar to those found in Jupiter's magnetosheath explored by the Ulysses flyby (Bolzan and Echer, 2014). The magnetic field components in that interval were found to have a power spectrum following a power law of about −2.1 to −2.2, similar to what is observed in the Neptune's magnetosheath (present work). For the Saturn's magnetosheath, Hadid et al. (2015) found fluctuations with index of −1.0 at the MHD scales, and −2.6 at the sub-ion scales.

For the Earth's magnetosheath, results from the Multiscale Mission showed that, from the subsolar region to the flanks of the magnetosheath, the spectral index of magnetic field spectra at MHD scales changed from ∼ 2.0 to

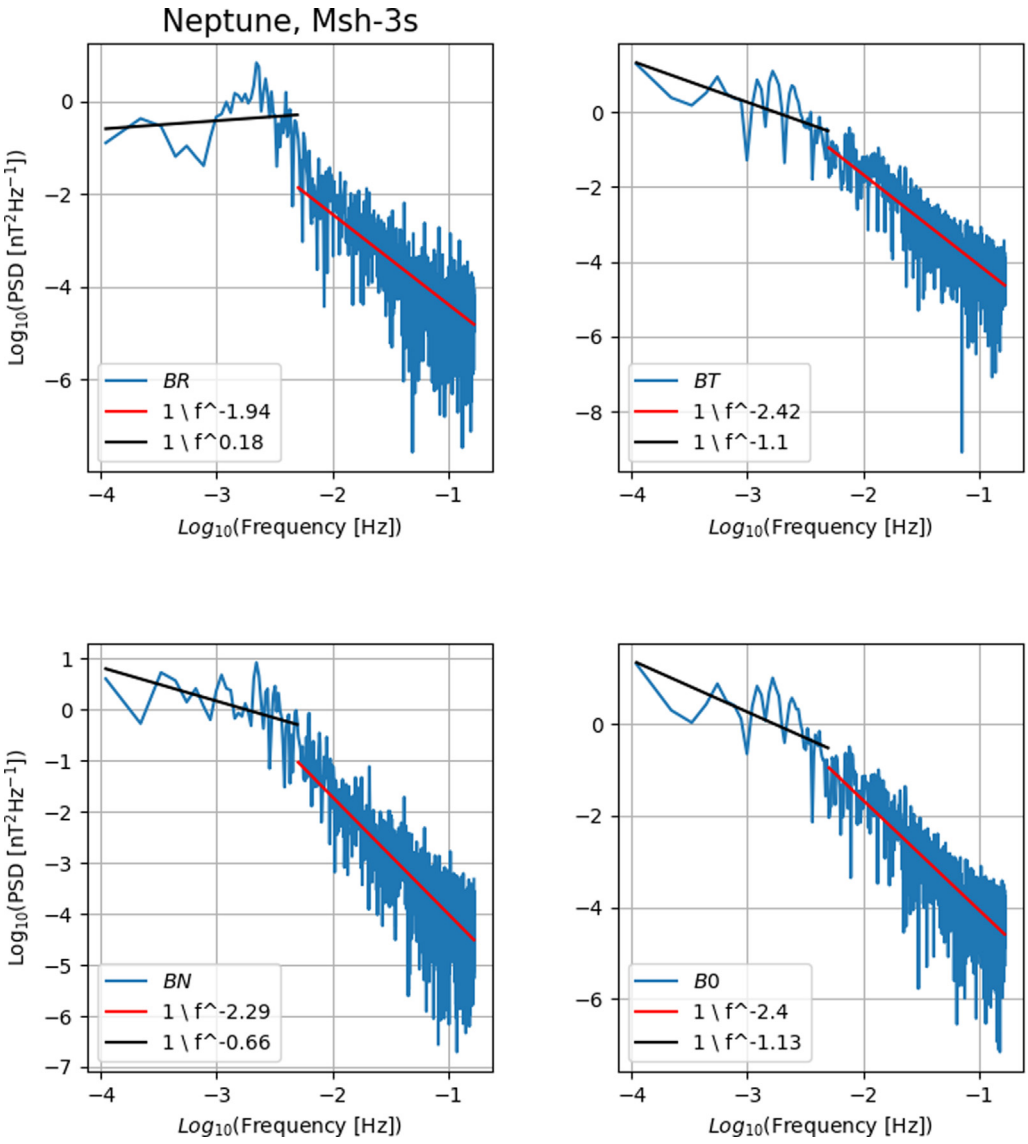

Fig. 4. Fourier power spectrum (blue line) and power law fit (black lines for the low frequency and red lines for the high-frequency ranges) of the magnetic field vector components and magnitude during the magnetosheath interval. (For interpretation of the references to colour in this figure legend, the reader is referred to the web version of this article.)

−1.5, with a positive correlation with the Alfvén Mach number (Li et al., 2020).

Echer and Bolzan (2016) studied the solar wind and waves upstream the Uranus' magnetosphere. They found that for the solar wind the magnetic field components follow a power law of about −1.4 to −1.7, which was lower (in absolute value) than the foreshock wave intervals (−1.8 to −2.0). The magnetosheath power law found in this and in previously cited works have a power law index much higher (again in absolute values) than that background solar wind, and similar or higher than the foreshock ones.

Fig. 5 shows the computed kurtosis parameters of the magnetic field magnitude and vector components in the magnetosheath. The kurtosis was computed every 5 min, from 5 to 65 minute scales.

It can be seen that kurtosis is higher than 3 for the B_R and B_N components in almost all scales except in 5 and 55 minutes for B_N and in 60 minutes for B_R. The B_T component presents values of kurtosis near 3 for the 5 and 40 minute scales, and it is slightly below 3 in the 25 minutes scale (2.9). Gaussian distribution was observed in the 20 minutes scale. In the magnetic field magnitude, the kurtosis parameter presents value very close to 3 for the 40 minutes scale. A Gaussian distribution was observed in the 20 minutes scale, as it was seen for B_T component. Further, the kurtosis is slightly below 3 for the 25 minutes scale, showing the same value that was found for B_T component (2.9). As this direction is where most of the field is aligned, this means that the kurtosis and intermittence are higher in the transverse than in the longitudinal field components. The higher value of kurtosis (6.5) is seen for B_N component at scale of

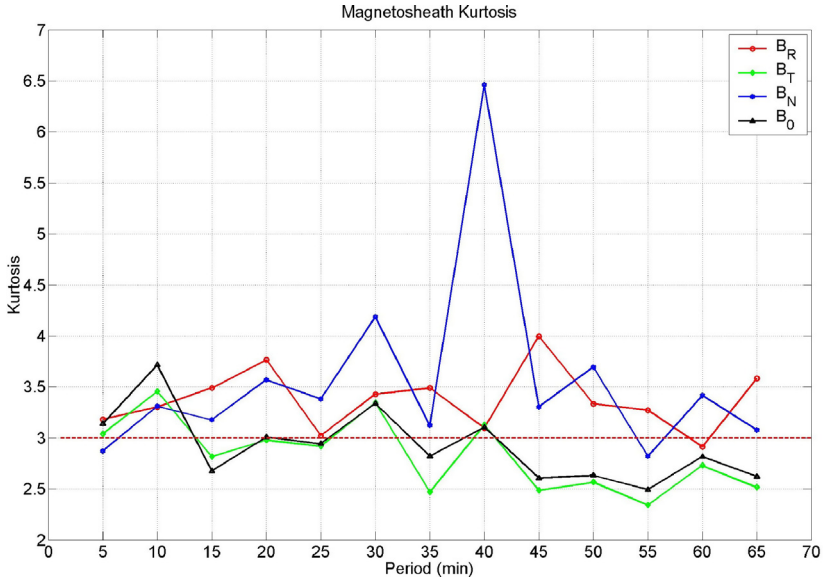

Fig. 5. Kurtosis values for the magnetosheath magnetic field components: B_R (red), B_T (green), B_N (blue) and magnitude B_0 (black). (For interpretation of the references to colour in this figure legend, the reader is referred to the web version of this article.)

40 minutes. For B_R component kurtosis is enhanced in short scales from 5 to 20 minutes, coherent with the predominance of this short period or high frequency oscillations in its spectrum. The higher value of kurtosis in the B_R component is observed in the 45 minutes scale, close to the peak observed in the B_N. While the B_N kurtosis peak at period of 40 minutes is also corresponding to the strong power seen in this low frequency part of its spectrum, as shown in Fig. 3. In the total field, the higher value of kurtosis, 3.7 was found in the 5 minutes scale.

The results are consistent with those obtained by the Lomb-Scargle analysis (present work), as well as with the results obtained through the wavelet analysis by Echer (2009). The major peak at about 40 minutes in kurtosis and spectral power is related to the dominant wave periodicity in the second half of the magnetosheath to the magnetopause. The short-term periods, 5 to 15 minutes, with high kurtosis are found mainly near the bow shock. The 20 to 30 minute oscillations have lower values of kurtosis and of spectral power. Those periodical oscillations were found in previous work (Echer, 2009) to be located close to the magnetopause where the intermittence of the magnetosheath is smaller and plasma structures are better organized.

For comparison, in the Jupiter's magnetosheath, Bolzan and Echer (2014) noted that all the magnetic field components presented higher values of the kurtosis to small scale (2 seconds) showing the presence of strong intermittence in this scale. Here, we also observed higher values for small scales, except for the B_N component. In the Uranus space environment, Echer and Bolzan (2016) have found kurtosis values below or near 3 for the background solar wind, and slightly higher than 3 for most of the frequencies in the foreshock wave interval.

3.4. Multifractal analysis

The magnetosheath magnetic field turbulence is further studied by the multifractal analysis shown in Fig. 6. It can be seen that the magnetosheath fluctuations show a singularity spectrum, approximately an upside-down parabola, with peaks at $f(\alpha_{max})$ and an extensive range of the α value. The singularity spectra are found to be widely spread. The result can be interpreted as a manifestation of strong multifractality and a complex plasma fluid dynamics in the magnetosheath.

For comparison, we also show the singularity spectrum obtained using the p-model (blue curve). It can be noted

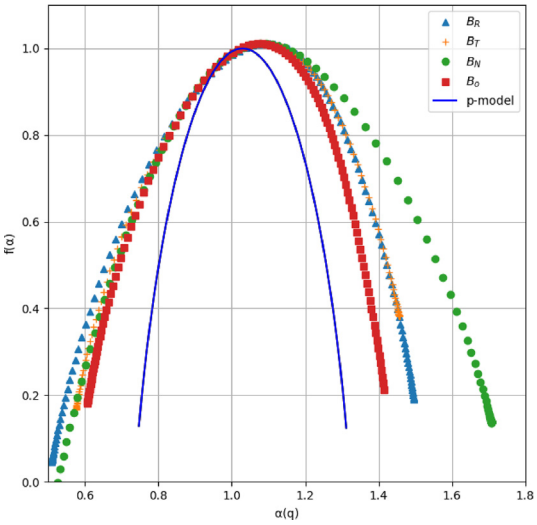

Fig. 6. Singularity spectra of magnetosheath magnetic field components and magnitude. The p-model curve is shown by the blue line curve. (For interpretation of the references to colour in this figure legend, the reader is referred to the web version of this article.)

that the values of the μ parameter are higher for the magnetosheath data than for the p-model curve, indicating a high level of intermittence in the magnetosheath magnetic field. The $f(\alpha)$ spectra for the magnetosheath are of non-parabolic shapes, deviating from the p-model. The smaller values of α correspond to the events occurring in bursts, while higher values of α correspond to events occurring sparsely (Bolzan et al., 2009).

From Fig. 6 it can be noted that the B_N component presented a long range of the α values, i.e., B_N presented a more spread parabolic shape, indicating a strong intermittence due the μ value and corroborating results from the kurtosis parameter (Fig. 5). Thus, we observe that the B_N component has higher values for the kurtosis at 40 minutes, and in the multifractal spectrum high values of α, indicating probably the presence of the coherent structures. This result is consistent with our previous work where we have also reported coherent structures in the Jupiter's magnetosheath (Bolzan and Echer, 2014).

4. Summary and conclusions

The turbulence in the Neptune's dayside magnetosheath magnetic field is studied using multiple statistical techniques. The main results are summarized below.

1. Neptune's bow shock was found to be quasi-perpendicular (with the shock angle θ_{Bn} of 57°) and strong (with the magnetic field compression ratio r_B of 3.1), in agreement with previous works.
2. The fluctuations in the magnetosheath have higher-frequency periods, observed mainly in the B_R component (about 4–7 minutes), while lower-frequency, large-amplitude oscillations of about 30–50 and 25–40 minutes are predominant in the B_T and B_N components, respectively. This result is in agreement with previous results (Echer, 2009).
3. From the Fourier analysis, it was found that the spectral index for frequencies higher than 0.00165 Hz was larger than −2 in the magnetosheath. This indicates a steep spectrum and a high energy transfer from large to small scales in the magnetosheath, leading to intense turbulent activity. These values are similar to those observed in other planetary magnetosheaths.
4. The statistical kurtosis values for B_R and B_N were higher than 3 in almost all scales, while the B_T component (main field direction) had a more Gaussian or sub-Gaussian behavior, specially in scales higher than 20 minutes. In particular, the B_N component presented high values of kurtosis for the time scale of $\sim$ 40 minutes associated with the low-frequency oscillations in the magnetic field. This result indicates an asymmetric or non-Gaussian magnetic field distribution in the Neptune's magnetosheath.
5. From the multifractal analysis, the singularity spectra were found to be more spread due to the higher coefficient μ values in the magnetosheath showing the richness and complexity of dynamics there. It can be noted that the multifractal results corroborate the results from kurtosis analysis, and the Lomb-Scargle power spectra showing the higher power peak at 40 minutes period. The larger spread observed in the B_N component in the multifractal spectrum is likely due to the peak of kurtosis at the high power low-frequency 40 minute period.

In this work, we have applied several statistical data analysis techniques in order to study the turbulence in the dayside magnetosheath of Neptune probed by the Voyager-2 spacecraft. Overall, strong plasma turbulence activity was found in the magnetosheath which is most likely due to ion-cyclotron waves.

From these results it seems that in the Neptune's dayside magnetosheath there are both compression and transverse fluctuation waves. The intermittence given by kurtosis show high values at high frequency for the B_R component and at low frequencies for B_N component. On the other hand, the power law analysis showed higher power index for the B_T component and the field magnitude, indicating a steep spectrum and large energy transfer from large to small time scales. However, the power index for transverse fluctuations is also high. In the original data it is possible to see fluctuations in all components. While for the B_T component (along the field direction) these fluctuations are about up to 50% of the field value or about $0.5B_0$. On the other hand, for the transverse components they can be relatively higher, as their average values are small (close to zero). These main periods are much longer than the proton gyro period of about 1.5 minutes, thus these waves can be considered to be in the MHD regime.

Theoretical work on the MHD turbulence cascading has been done in the last decades (Goldreich and Sridhar, 1997; Oughton and Matthaeus, 2005; Zank and Matthaeus, 1993b; Zank and Matthaeus, 1993a). Goldreich and Sridhar (1997) analysed the nature of nonlinear couplings between colliding Alfvén waves. They found a new type of turbulence, the intermediate turbulence, at which scale the cascade of energy in the inertial range exhibits properties intermediate between those of weak and strong turbulent cascades. Oughton and Matthaeus (2005) discussed the distinct nature of parallel and perpendicular cascades and their roles in the evolution of solar wind fluctuations. Zank and Matthaeus (1993a) presented a new model for the investigation of waves and turbulence in the solar wind, which treats the effects of both compressibility and incompressibility.

For higher spectral index, the power spectrum is steeper. This implies a fast change of power of the oscillations with frequency (fast decreases with increasing frequency). It can be interpreted as a fast decrease of energy of the system from large scales to small scales. Therefore, for higher spectral index there will be faster energy transfer.

An interesting topic to explore in future works is to compare the turbulent activity in the magnetosheaths of

the four outer planets (Bolzan and Echer, 2014; Saur, 2021).

Finally, this kind of study can be of interest for possible future missions to the Neptune system, which would explore in larger detail the Neptune's magnetosphere and its moons (Kollmann, 2020).

Declaration of Competing Interest

The authors declare that they have no known competing financial interests or personal relationships that could have appeared to influence the work reported in this paper.

Acknowledgments

E. E. would like to thank Brazilian agencies for research grants: CNPq (contract No. PQ-302583/2015–7, PQ-301883/2019–0, PQ-300160/2021–6) and FAPESP (2018/21657–1). The work of R. H. is funded by the Science and Engineering Research Board (SERB, Grant No. SB/S2/RJN-080/2018), a statutory body of the Department of Science and Technology (DST), Government of India through a Ramanujan fellowship. The work of A. M. S. F. is funded by the Brazilian CNPq agency (project No. PQ-300969/2020–1, PQ-301542/2021–0). The work of M. J. A. B. was supported by CNPq agency (contract No. PQ-302330/2015–1, PQ-305692/2018–6) and FAPEG agency (contract No. 2012.1026.7000905). We thank the Brazilian Ministry of Science, Technology and Innovation and the Brazilian Space Agency as well. The Voyager-2 plasma and magnetic field data used in this work are obtained from the Planetary Data System (https://pds.nasa.gov/).

References

Arneodo, A., Bacry, E., Muzy, J.F., 1995. The thermodynamics of fractals revisited with wavelets. Phys. A 213, 232–275.

Baluev, R.V., 2008. Assessing the statistical significance of periodogram peaks. Mon. Not. R. Astron. Soc. 385 (3), 1279–1285. https://doi.org/10.1111/j.1365-2966.2008.12689.x.

Behannon, K., Acuna, M., Burlaga, E.A., L.F., 1977. Magnetic field experiments for voyagers 1 and 2. Space Sci. Rev., 21, 235–257.

Bittencourt, J.A., 2010. Fundamentals of plasma physics. In: Fundamentals of Plasma Physics. Springer, p. (p. 679)..

Bolzan, M.J.A., Echer, E., 2014. A multifractal approach applied to the magnetic field turbulence in jupiter's magnetosheath. Planet. Space Sci. 91, 77–82.

Bolzan, M.J.A., Rosa, R.R., Sahai, Y., 2009. Multifractal analysis of low-latitude geomagnetic fluctuations. Ann. Geophys. 27, 569–576.

Bolzan, M.J.A., Tardelli, A., Pillat, V.G., et al., 2013. Multifractal analysis of vertical total electron content (vtec) at equatorial region and low latitude, during low solar activity. Ann. Geophys. 31, 127–133.

Bracewell, R.N., 2014. The Fourier Transform and Its Applications, 3rd ed. CBS Publishers & Distributors Pvt. Ltd.

Chhiber, R., Matthaeus, W.H., Bowen, T.A., et al., 2021. Subproton-scale intermittency in near-sun solar wind turbulence observed by the parker solar probe. Astrophys. J. Lett. 911, 1–6.

Cuesta, M.E., Parashar, T.N., Chhiber, R., et al., 2022. Intermittency in the expanding solar wind: Observations from parker solar probe (0.16 au), helios 1 (0.3–1 au), and voyager 1 (1–10 au). Astrophys. J. Suppl. Series 259, 1–16.

Davis, J.C., 2002. Statistics and data analysis in geology. In: Statistics and Data Analysis in Geology. Wiley.

Echer, E., 2009. Foreshock and magnetosheath waves at uranus and neptune studied with wavelet analysis. Adv. Space Res. 44, 1030–1037.

Echer, E., 2019. Solar wind and interplanetary shock parameters near saturn's orbit (~10 au). Planet. Space Sci. 165, 210–220.

Echer, E., Bolzan, M.J.A., 2016. A comparative study of solar wind and foreshock turbulence near uranus orbit. Planet. Space Sci. 120, 70–77.

Fairfield, D., 1976. Magnetic fields of the magnetosheath. Rev. Geophys. 14, 117–134.

Franco, A.M.S., Franz, M., Echer, E., et al., 2020. Wavelet analysis of low frequency plasma oscillations in the magnetosheath of mars. Adv. Space Res. 65, 2090–2098.

Franco, A.M.S., Hajra, H., Echer, E., et al., 2021. Seasonal features of geomagnetic activity: a study on the solar activity dependence. Ann. Geophys. (pp –).

Frisch, U., 1995. Turbulence: The Legacy of AN Kolmogorov. Cambridge University Press.

Goldreich, P., Sridhar, S., 1997. Magnetohydrodynamic turbulence revisited. Astrophys. J. 485, 680.

Hadid, L.Z., Sahraoui, F., Kiyani, K.H., et al., 2015. Nature of the mhd and kinetic scale turbulence in the magnetosheath of saturn: Cassini observations. Astrophys. J. Lett. 813, L29.

Hajra, R., Franco, A.M.S., Echer, E., et al., 2021. Long-term variations of the geomagnetic activity: a comparison between the strong and weak solar activity cycles and implications for the space climate. J. Geophys. Res. Space Phys. 126. https://doi.org/10.1029/2020JA028695, e2020JA028695.

Halsey, T.C., Jensen, M.H., Kadanoff, L.P., et al., 2018. Fractal measures and their singularities: The characterization of strange sets. Phys. Rev. A 33 (2), 1141–1151. https://doi.org/10.1103/PhysRevA.33.1141.

Hasegawa, A., 1969. Drift mirror instability in the magnetosphere. Phys. Fluids 12, 2642–2650.

Horne, J.H., Baliunas, S.L., 1986. A prescription for period analysis of unevenly sampled time series. Astrophys. J. 302, 757. https://doi.org/10.1086/164037.

Iroshnikov, P.S., 1963. Turbulence of a conducting fluid in a strong magnetic field. Astron. Zh. 40, 742.

Kivelson, M.G., Bagenal, F., 1999. Planetary magnetospheres. Encycl. Res. 104, 469–492.

Kollmann, P.E.A., 2020. Magnetospheric studies: A requirement for addressing interdisciplinary mysteries in the ice giant systems. Space Sci. Rev. 216, 1–26.

Kolmogorov, A.N., 1941. Dissipation of energy in the locally isotropic turbulence. Dokl. Akad. Nauk SSSR 30, 301–305.

Kolmogorov, A.N., 1962. A refinement of previous hypotheses concerning the local structure of turbulence in a viscous incompressible fluid at high reynolds number. J. Fluid Mech. 13, 82–85.

Kraichnan, R.H., 1965. Inertial-range spectrum of hydromagnetic turbulence. Phys. Fluids 8, 1385.

Li, H., Jiang, W., Wang, C., et al., 2020. Evolution of the Earth's Magnetosheath Turbulence: A Statistical Study Based on MMS Observations. Astrophys. J. Lett. 898 (L43), 1–10.

Lomb, N.R., 1976. Least-squares frequency analysis of unequally spaced data. APSS 39 (2), 447–462. https://doi.org/10.1007/BF00648343.

McMahon, S.K., 1996. Overview of planetary data system. Planet. Space Sci. 44, 3–12.

Meneaveau, C., Sreenivasan, K.R., 1987. Simple multifractal cascade model for fully developed turbulence. Phys. Rev. Lett. 59, 1424–1427.

Muzy, J.F., Bacry, E., Arneodo, A., 1991. Wavelets and multifractal formalism for singular signals: Application to turbulence data. Phys. Rev. Lett. 67, 3515–3518.

Ness, N.F., Acuña, M.H., Burlaga, L.F., et al., 1989. Magnetic fields at neptune. Science 246, 1473–1478.

Obukhov, A.M., 1962. Some specific features of atmospheric turbulence. J. Geophys. Res. 67, 3011–3014.

Oswiecimka, P., Kwapien, J., Drozdz, S., 2006. Wavelet versus detrended fluctuation analysis of multifractal structures. Phys. Rev. E 74, 016103. https://doi.org/10.1103/PhysRevE.74.016103.

Oughton, S., Matthaeus, W.H., 2005. Parallel and perpendicular cascades in solar wind turbulence. Nonlinear Process. Geophys. 12, 299–310.

Press, W.H., Rybicki, G.B., 1989. Fast algorithm for spectral analysis of unevenly sampled data. Astrophys. J. 338, 277. https://doi.org/10.1086/167197.

Remya, B., Reddy, R.V., Tsurutani, B.T., et al., 2013. Ion temperature anisotropy instabilities in planetary magnetosheaths. J. Geophys. Res. 118, 785–793.

Richardson, J.D., 2002. The magnetosheaths of the outer planets. Planet. Space Sci. 50, 503–517.

Richardson, J.D., Stahara, S.S., Siscoe, G.L., et al., 1994. The magnetosheath of neptune: models and observations. J. Geophys. Res. 99, 14789–14797.

Russell, C.T., Luhmann, J.G., 1997. Neptune: magnetic field and magnetosphere. In: Shirley, J.H., Fainbridge, R.W. (Eds.), Encyclopedia of Planetary Sciences. Champan & Hall, New York, p. (p. 533)..

Russell, C.T., Walker, J.R., 1995. The magnetospheres of the outer planets. In: Kivelson, M.G., Russell, C.R. (Eds.), Introduction to Space Physics. Cambridge University Press, Cambridge, pp. 503–520.

Saur, J., 2021. Turbulence in the magnetospheres of the outer planets. Front. Astron. Space Sci. 8, 1–6.

Scargle, J.D., 1982. Studies in astronomical time series analysis. II. Statistical aspects of spectral analysis of unevenly spaced data. Astron. J. 263, 835–853. https://doi.org/10.1086/160554.

Szabo, A., Lepping, R.P., 1995. Neptune inbound bow shock. J. Geophys. Res. 100, 1723–1730.

Tsurutani, B., Lakhina, G.S., 1997. Some basic concepts of wave-particle interactions in collisionless plasmas. Rev. Geophys. 35, 491–501.

Tsurutani, B.T., Lakhina, G.S., Verkhoglyadova, O.P., et al., 2011. Magnetosheath and heliosheath mirror mode structures, interplanetary magnetic decreases, and linear magnetic decreases: Differences and distinguishing features. J. Geophys. Res. 116, 1.

Tsurutani, B.T., Smith, E.J., Anderson, R.R., et al., 1982. Lion roars and nonoscillatory drift mirror waves in the magnetosheath. J. Geophys. Res. 87, 6060–6072.

VanderPlas, J.T., 2018. Understanding the Lomb-Scargle Periodogram. Astrophys. J. Suppl. Series 236 (1), 16. https://doi.org/10.3847/1538-4365/aab766.

VanderPlas, J.T., Ivezić, Ž., 2015. Periodograms for multiband astronomical time series. Astrophys. J. 812 (1), 18. https://doi.org/10.1088/0004-637X/812/1/18.

Wan, M., Matthaeus, W., Roytershteyn, V., et al., 2016. Intermittency, coherent structures and dissipation in plasma turbulence. Phys. Plasmas 23 (4). https://doi.org/10.1063/1.4945631.

Zank, G.P., Matthaeus, W.H., 1993a. Nearly incompressible fluids. II: Magnetohydrodynamics, turbulence, and waves. Phys. Fluids A: Fluid Dyn. 5, 257.

Zank, G.P., Matthaeus, W.H., 1993b. Waves and turbulence in the solar wind. J. Geophys. Res. 97, 17189–17194.

Zechmeister, M., Kürster, M., 2009. The generalised Lomb-Scargle periodogram. A new formalism for the floating-mean and Keplerian periodograms. Astron. Astrophys. 496 (2), 577–584. https://doi.org/10.1051/0004-6361:200811296.

Zhang, M., Belcher, J.W., McNutt Jr, R., 1992. Plasma observations near neptune: results from voyager-2. Adv. Space Res. 12, 37–46.

Zhang, M., Richardson, J.D., Sittler, E.C., 1991. Voyager 2 electron observations in the magnetosphere of neptune. J. Geophys. Res. 96, 19085–19100.